High-efficiency blazed transmission gratings for high-resolution soft x-ray spectroscopy

Ralf K. Heilmann,[1] Alexander R. Bruccoleri,[2] and Mark L. Schattenburg,[1]

[1]Space Nanotechnology Laboratory, MIT Kavli Institute for Astrophysics and Space Research, Massachusetts Institute of Technology, Cambridge, Massachusetts 02139, USA
[2]Izentis LLC, 303 3rd St. #101, Cambridge, MA 02142, USA

ABSTRACT

High-resolution spectroscopy of astrophysical sources is the key to gaining a quantitative understanding of the history, dynamics, and current conditions of the cosmos. A large-area ($>$ 1,000 cm^2), high resolving power ($R = \lambda/\Delta\lambda > 3000$) soft x-ray grating spectrometer (XGS) that covers the lines of C, N, O, Ne and Fe ions is the ideal tool to address a number of high-priority science questions from the 2010 Decadal Survey, such as the connection between super-massive black holes and large-scale structure via cosmic feedback, the evolution of large-scale structure, the behavior of matter at high densities, and the conditions close to black holes. While no grating missions or instruments are currently approved, an XGS aboard a potential future X-ray Surveyor could easily surpass the above performance metrics. To improve the chances for future soft x-ray grating spectroscopy missions or instruments, grating technology has to progress and advance to higher Technology Readiness Levels (TRLs). To that end we have developed Critical-Angle Transmission (CAT) gratings that combine the advantages of blazed reflection gratings (high efficiency, use of higher diffraction orders) with those of conventional transmission gratings (low mass, relaxed alignment tolerances and temperature requirements, high transparency at higher energies). A CAT grating-based spectrometer can provide performance 1-2 orders of magnitude better than current grating instruments on Chandra and Newton-XMM with minimal resource requirements. At present we have fabricated large-area freestanding CAT gratings with narrow integrated support structures from silicon-on-insulator wafers using advanced lithography and a combination of deep reactive-ion and wet etching. Our latest x-ray test results show record high absolute diffraction efficiencies in blazed orders in excess of 30% with room for improvement.

Keywords: x-ray optics, critical-angle transmission grating, x-ray spectroscopy, blazed transmission grating, soft x-ray, silicon-on-insulator, deep reactive-ion etching

1. INTRODUCTION

The soft x-ray band contains the characteristic lines of highly ionized carbon, nitrogen, oxygen, neon and iron that are central to studies of the Warm Hot Intergalactic Medium, the search for the missing baryons, the study of the outflows of supermassive black holes and the properties of galaxy halos. Soft x-ray plasma diagnostics also provide crucial information about the evolution of large scale structure and cosmic feedback. In addition, soft x-ray spectroscopy of individual stars can help to reveal the effects of rotation, magnetic fields and stellar winds in stellar coronae. See for example Bautz *et al.*[1] and references therein. These topics include high-priority science questions identified in the Astro2010 Decadal Survey "New Worlds New Horizons" (NWNH),[2] as well as in the 2013 "Enduring Quests, Daring Visions" visionary Astrophysics Roadmap.[3]

Today's x-ray grating spectrometer (XGS) instruments (the HETGS[4] on Chandra and the RGS[5] on XMM-Newton) were launched sixteen years ago, far exceeding their expected lifetimes. They are based on technology from the 80's and early 90's and underperform by 1-2 orders of magnitude compared to what is possible today and required to address the above science questions. For future XGS instruments high collecting area ($>$ 1000 cm^2) and high resolving power ($R = \lambda/\Delta\lambda > 3000$) need to go hand in hand - one is of limited use without the other.

Further author information: Send correspondence to R.K.H. E-mail: ralf@space.mit.edu, URL: http://snl.mit.edu/home/ralf

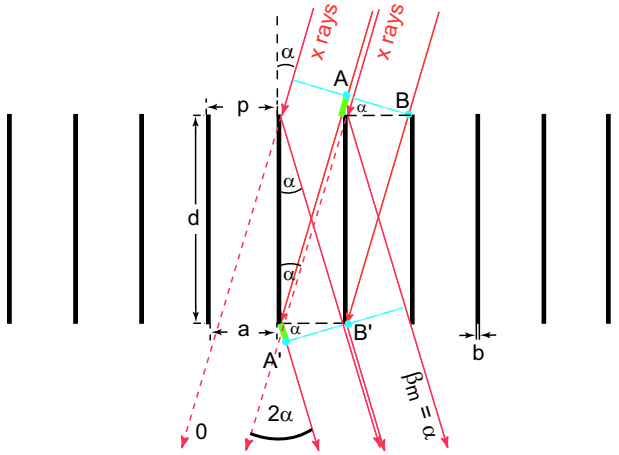

Figure 1. Schematic cross section through a CAT grating of period p. The m^{th} diffraction order occurs at an angle β_m where the path length difference between AA' and BB' is $m\lambda$. Shown is the case where β_m coincides with the direction of specular reflection from the grating bar side walls ($\beta_m = \alpha$), i.e., blazing in the m^{th}order.

Many recently developed mission concepts for a soft x-ray spectrometer, either as a dedicated spectroscopy mission,[1,6–9] or as an instrument on board a larger x-ray observatory,[8,10–14] have demonstrated the feasibility of meeting area and resolving power requirements once technologies in the areas of x-ray mirrors and x-ray gratings have achieved sufficient Technology Readiness Levels (TRLs).

In preparation for the 2020 Decadal Survey, which will be tasked to prioritize large missions to follow JWST and WFIRST, NASA plans to provide information on several large mission concepts.[15] One of these mission concepts might be a so-called X-ray Surveyor from the visionary roadmap.[3] An informal X-ray Surveyor mission concept team recently has put together a baseline mission concept assuming a telescope with sub-arcsecond angular resolution and square-meter collecting area. A microcalorimeter ($\Delta E < 5$ eV) and a wide field-of-view, small pixel imager are envisioned at the focus, and a retractable soft x-ray grating spectrometer (with a readout array in the focal plane) can provide $R = \lambda/\Delta\lambda$ on the order of 5,000, with an effective area of $\sim 4,000$ cm^2.[16,17] Due to the high transparency of transmission gratings at higher energies an XGS based on Critical-Angle Transmission (CAT) gratings would work in perfect synergy with a microcalorimeter at the focus, allowing for simultaneous high spectral resolution observations over the 0.2 - 10 keV range with maximum collecting area.

X-ray transmission gratings offer low mass and relaxed, easily achievable alignment requirements compared to reflection gratings. These properties alone minimize resource requirements due to lower mass support structures and increased tolerance for temperature variations. In addition, CAT gratings promise high diffraction efficiencies and the ability to blaze in higher orders, comparable to the most advanced reflection grating designs.

We briefly describe the CAT grating principle below. We then present our progress in CAT grating fabrication and recent x-ray efficiency measurements and discuss our future plans.

2. CAT GRATING PRINCIPLE

Critical-angle transmission (CAT) gratings are freestanding transmission gratings with ultra-high aspect-ratio grating bars. They can be described as blazed transmission gratings and combine the advantages of past-generation transmission and blazed reflection gratings.[18–21] The basic structure of a CAT grating is shown in Fig. 1 in cross section. X rays are incident onto the nm-smooth side walls of thin, ultra-high aspect-ratio grating bars at an angle α below the critical angle for total external reflection, θ_c (e.g., $\theta_c = 1.7°$ for 1 keV photons reflecting off a silicon surface). For optimum efficiency the grating depth $d = a/\tan\alpha$ (a being the spacing between two adjacent grating bars), the grating bar thickness b should be as small as possible, and the gratings should be freestanding. Diffraction orders appear at angles given by the grating equation

$$\frac{m\lambda}{p} = \sin\alpha - \sin\beta_m, \tag{1}$$

with $m = 0, \pm1, \pm2, ...$, λ being the x-ray wavelength, and p being the grating period.

We have previously fabricated small CAT grating prototypes with periods of 574[20–22] and 200 nm[11,18,21,23,24] with anisotropic wet etching of lithographically patterned <110> silicon-on-insulator (SOI) wafers in potassium hydroxide (KOH) solutions. We have achieved small grating bar duty cycles ($b/p < 20\%$), unprecedented grating bar aspect ratios (d/b up to 150), and smooth side walls. X-ray tests have shown that these wet-etched grating prototypes perform at the level of 50-100% of theoretical predictions for ideal CAT gratings over a broad wavelength band.[18,20] However, due to the large loss of grating area to the unavoidable widening of the cross-support mesh bars in the wet-etch process the absolute diffraction efficiency remained mostly in the 5-15% range.[18]

3. CAT GRATING FABRICATION

The building of a large-area grating array requires structural definition over at least nine orders of magnitude - from nanometer-smooth side walls to meter-scale grating array structures. We briefly describe the main structures, and then focus on the current state of the nanofabrication process for cm^2-sized CAT grating membranes.

3.1 Large-area CAT grating arrays

Thin membranes containing CAT grating structures are fabricated from silicon-on-insulator (SOI) wafers, where the device layer thickness determines the depth of the grating. In order to build large-area ($\sim m^2$) grating arrays the grating membranes are mounted onto thin machined frames, resulting in a flat grating facet ($\sim 30\times30$ mm^2 to 60×60 mm^2 in size). Facets in turn are tiled over large areas by mounting them to large grating array structures shaped according to the CAT-XGS optical design.

3.2 Membrane structural hierarchy

The very fine CAT grating bars need to be supported in order to prevent them from bending and sticking to each other. For that purpose we have introduced an integrated so-called Level 1 (L1) cross support mesh that is etched out of the SOI device layer at the same time as the CAT grating bars. We use the much thicker SOI handle layer to separately etch out a high-throughput hexagonal Level 2 (L2) mesh that gives the thin device layer the necessary mechanical strength for a large-area membrane. Fig. 2 gives a schematic representation of the structural hierarchy.

3.3 Nanofabrication

We give a top level overview of our current sequence of process steps to fabricate CAT grating membranes. Details on many of these steps can be found in the literature.[22,23,27–30]

Anisotropic etching in KOH can lead to very smooth grating bar sidewalls if the mask grating pattern is well-aligned to the silicon {111} planes that run normal to the <110> SOI wafer. However, as alluded to above, inclined {111} planes are protected by the orthogonal L1 mesh mask, which leads to trapeziodally widening L1 bars with increasing etch depth. Our approach to solve this problem has been to first perform a highly anisotropic deep etch with a crystal-lattice-independent deep reactive-ion etch (DRIE) to transfer the combined CAT grating and L1 pattern into the SOI device layer simultaneously. DRIE leaves the sidewalls rough, so we follow up with a short wet etch in KOH solution.[30]

Fig. 3 shows the main process steps. We begin with an SOI wafer with 300 nm of thermal oxide on it and add a 4 micron thick layer of PECVD (plasma-enhanced chemical vapor deposition) silicon oxide to the back side. The back side is patterned using photoresist and contact lithography. We then pattern the front (device layer) side with two interference lithography steps (using a combination of chrome, anti-reflection coating, tantalum and silicon oxide and photoresist as mask layers). For the correct alignment of the interference fringes to the {111} planes we first find the orientation of these planes using a series of steps described previously,[30] since relying on wafer flats is not accurate enough.

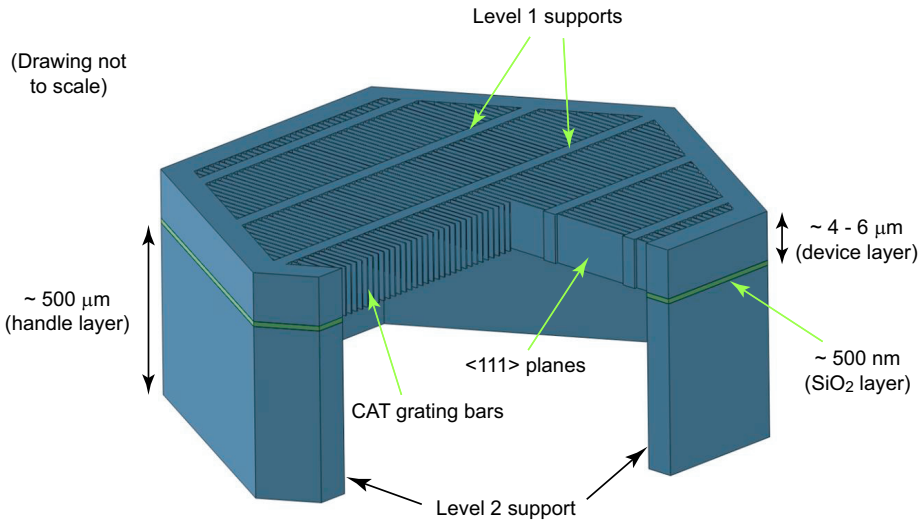

Figure 2. Schematic of a grating membrane "unit cell" (not to scale), formed by a single L2 support mesh hexagon. The L2 mesh is etched out of the SOI handle layer (back side). The device layer contains the fine-period CAT grating bars and in the perpendicular direction the coarse, low duty cycle integrated L1 support mesh. Device and handle layers are separated by the thin buried silicon oxide layer that serves as an etch stop for both front and back side etches.

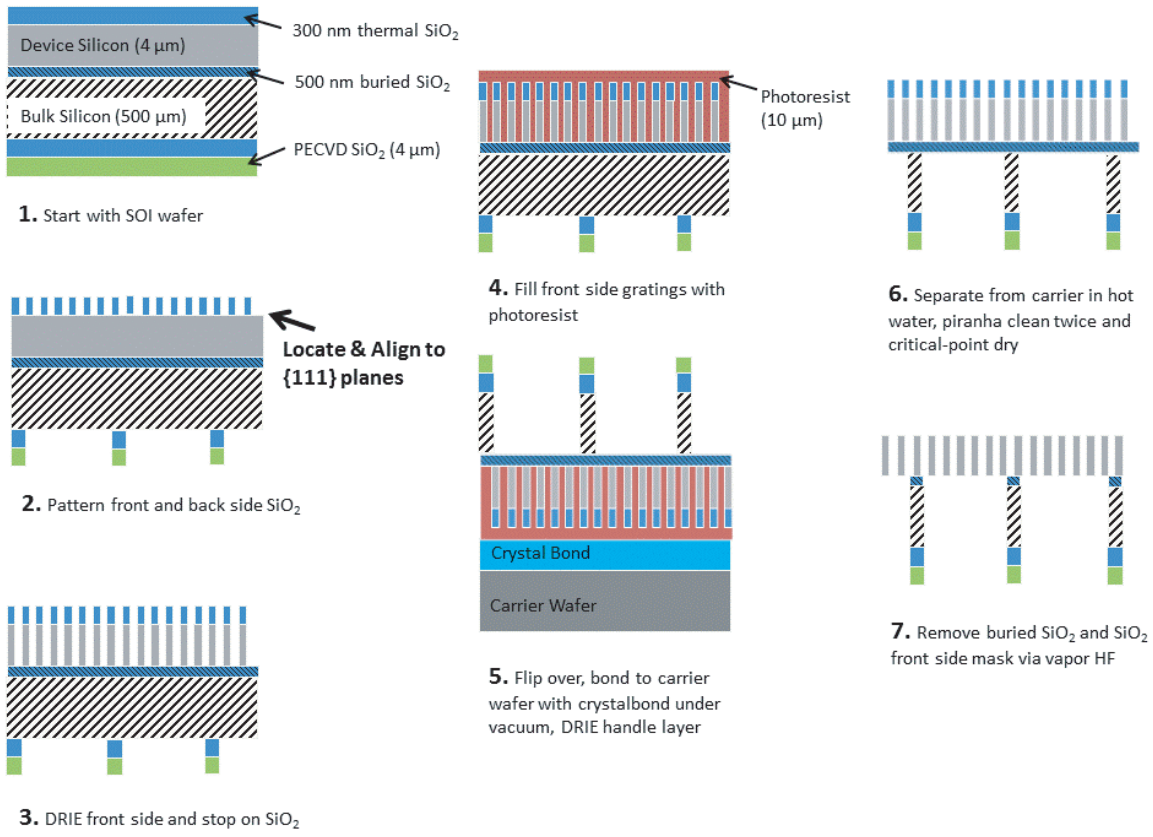

Figure 3. Schematic of top level CAT grating membrane fabrication steps. The wet etch in KOH solution takes place between steps 3 and 4.

The resulting combined pattern of CAT grating and L1 support bars is then transferred into the thermal oxide, which serves as the etch mask for the subsequent DRIE step. DRIE stops on the buried oxide (BOX) layer. A lot of process development went into achieving high quality grating bar profiles with minimal bowing or scalloping (see Fig. 4), which only became possible after we were able to acquire a dedicated DRIE tool.[30,31] We then immerse the sample in KOH solution for a timed wet etch to "polish" the rough grating bar sidewalls, which are nominally parallel to {111} silicon crystal planes. Next the grating is filled with photoresist for protection.

Now that the grating is protected we flip the wafer over and bond it under vacuum to a carrier wafer with crystalbond. We then DRIE the back side hexagons out of the handle layer, again stopping on the BOX layer. Of course the DRIE recipe for the back side etch is different from the one for the much more sensitive front side etch. The sample is then separated from the carrier in hot water and piranha cleaned twice to remove the resist from the grating. Initially this was followed by a wet etch in hydrofluoric acid (HF) to remove the BOX layer and the left-over oxide mask, but we found this process impractical and difficult to time (if the etch is too short the BOX layer is still there, if it is too long it can completely remove the oxide between the L1 and L2 structures and detach the device from the handle layer - see also Fig. 4). Instead we now remove the oxide with an HF vapor etch.

All the samples described below have a grating period of 200 nm, and the L1 and L2 mesh periods are 5 μm and 1 mm, respectively. The device layer thickness of all SOI wafers was 4 μm according to the vendor, and the handle layer was 0.5 mm thick. L2 hexagon walls are $\sim$ 100 μm thick. Fig. 4 shows a few scanning electron microscope (SEM) images from recent samples. The grating areas on the tested samples are about 33 mm long and 6-8 mm wide.

4. X-RAY MEASUREMENTS

We performed all of our x-ray measurements at beam line 6.3.2 of the Advanced Light Source (ALS) synchrotron at Lawrence Berkeley National Laboratory (LBNL). A monochromatic beam is incident on the sample at the center of a goniometer. A slit-covered photodiode mounted to an arm of the goniometer measures the transmitted intensity as a function of diffraction angle relative to the straight-through (0^{th} order) beam. The gratings are oriented such that the dispersion axis is perpendicular to the plane of the synchrotron (i.e., the grating bars run horizontally). We find the surface normal of a grating membrane through rotation of the grating around the horizontal axis in the grating membrane until positive and negative diffraction peaks of the same order have the same intensity. The grating is then rotated around the same axis by some desired angle α, resulting in blazing of the diffracted orders that are near the angle 2α from the 0^{th} transmitted order. Orders within a "blaze envelope" (centered near 2α) have enhanced diffraction intensity, where the width of this envelope is proportional to λ/a (see Fig. 5).

Over the last year and a half we have tested gratings from three separate batches with a nominal depth of $d = 4$ μm and $p = 200$ nm. The first batch (B1) was the first successful fabrication of a large-area grating membrane with freestanding CAT grating bars using the combination of front and backside DRIE with KOH polishing. It had many defects such as broken bars and bars that stuck together with their neighbors, but it was of high enough quality to show pronounced blazing (Fig. 5 in Ref. 31). However, the strongest blazed order had less than 8% diffraction efficiency, and there was significant intensity between the orders. The second batch used an improved and more gentle front side filling process (step 4 in Fig. 3), which practically eliminated defects otherwise visible after the front side cleaning step. Going from a wet HF etch (to remove the BOX and front side mask) to etching in HF vapor also improved our yields.

The best sample from this batch (B2) showed large areas without defects. However, the BOX layer etch had removed the oxide between the L1 and L2 meshes in many places, presumably leading to partial delamination of the device and handle layers and subsequent buckling of the device layer when the two layers reconnected via van-der-Waals forces. We measured buckling of the device layer membrane over individual L2 hexagons with a Wyco NT 9800 optical profiler and observed seemingly random buckling in both directions (towards and away from the handle layer) with amplitudes ranging from $\sim$ 200 nm (practically flat) to several microns (see Fig. 6). The transmission geometry is very forgiving in terms of grating misalignments, such that only the most severe buckling might begin to have a detrimental effect on the resolving power. However, the changing local surface

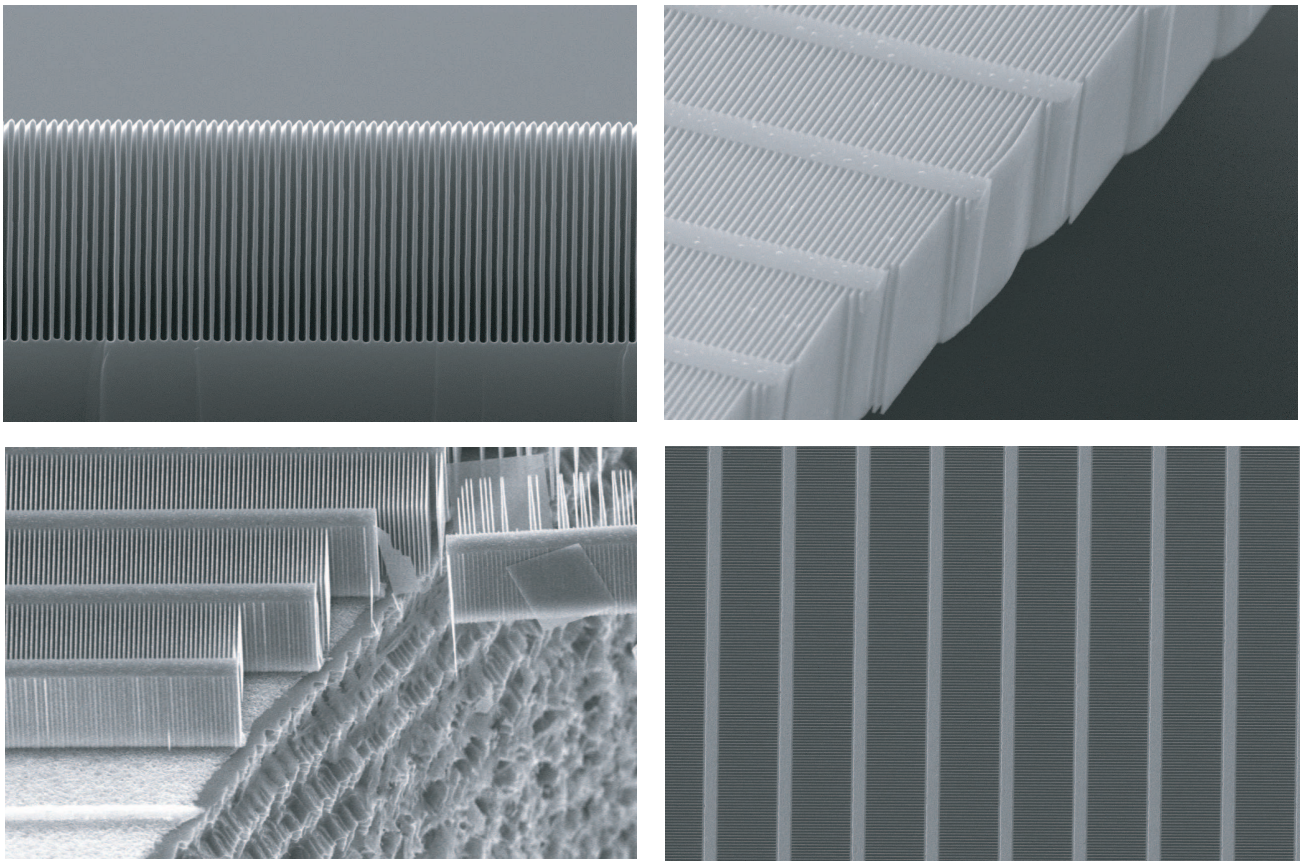

Figure 4. Scanning electron microscope images of recent samples. Top left: Cross section through device layer after DRIE/before KOH polishing, showing the high quality grating bar profile. Top right: Cleaved freestanding CAT grating membrane with low duty-cycle integrated L1 support mesh, etched for 7 minutes in KOH. Bottom left: Cleaved sample, showing the interface between the device layer (CAT grating and L1 supports after DRIE and KOH polish) on top of a L2 mesh bar that was etched from below, also with DRIE. Note the large wall roughness from the back side DRIE, and the leftover buried oxide that was protected by L2 and L1 meshes. Bottom right: Top view of a high-quality freestanding sample etched for 30 seconds in KOH, showing large defect-free areas. For all images CAT grating period is 200 nm, L1 mesh period is 5 μm, and the nominal device layer thickness is 4 μm.

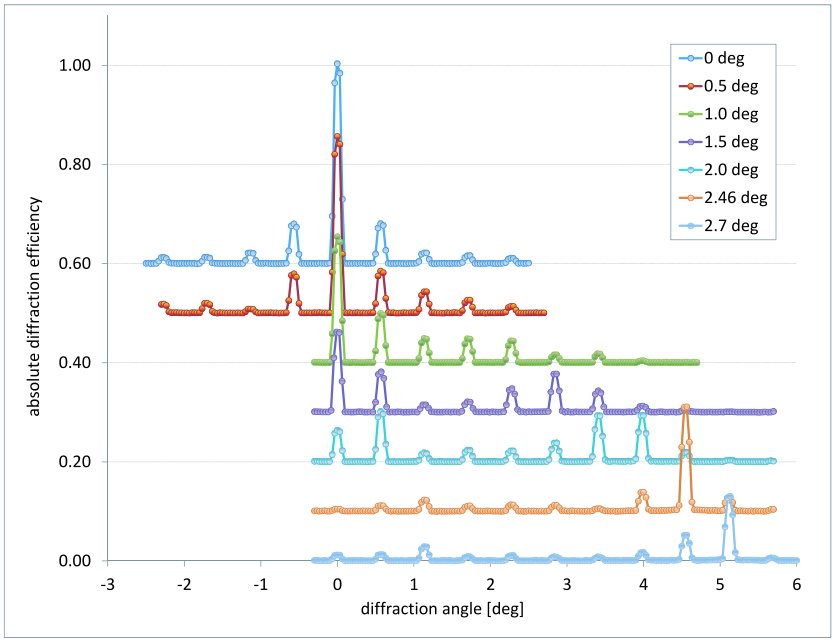

Figure 5. Absolute diffraction efficiency of sample S3 versus diffraction angle for a range of sample angles α relative to the incident x-ray beam with $\lambda = 2$ nm. Data sets are vertically offset for clarity. In the top data set diffraction peaks of the same order on each side of the 0^{th} order have the same intensity, signifying normal incidence. Tilting the sample by 0.5 deg (second data set from top) leads to an enhancement in intensity for orders 1-3 with positive diffraction angles relative to the same orders on the negative-angle side. Further tilting leads to increased diffraction intensity for even higher orders. Despite rotating the grating by several degrees, the changes in diffraction angles are much too small to be seen in this plot, demonstrating the relaxed alignment tolerances for transmission gratings in an XGS.

angles of a buckled hexagon relative to the incident beam can lead to angular shifts in the blaze envelope that weaken desired diffraction orders and strengthen others. This effect is more pronounced at shorter wavelengths due to the narrower blaze envelopes. The footprint of the x-ray beam (size $\sim 140 \times 360$ μm^2) on a buckled hexagon thus averages over a range of incidence angles, resulting in a reduced intensity for the nominally blazed diffraction orders. In Fig. 7(a) we compare the theoretical diffraction efficiency of the strongest blazed order for a perfect CAT grating (with geometrical parameters derived from SEM images) that also takes into account the effects of membrane curvature based on the measured buckling ("buckled model") with measured x-ray peak diffraction efficiencies. The comparison shows that the fabricated CAT grating delivers 60-95% of the peak diffraction efficiencies predicted by the buckled model. The shown absolute efficiencies are obtained simply by dividing the measured intensity by the intensity of the full beam incident on the detector. The efficiencies thus include absorption by the L1 mesh, since the beam averages over many L1 mesh periods. The model takes this into account, according to SEM measurements of L1 bar widths.

We tested four samples from the most recent batch, with the main difference between them being the amount of time they were etched in KOH. Sample S1 was etched for 30 sec in 10% KOH, sample S3 for 2 min in 25% KOH, sample S6 for 20 min in 50% KOH, and sample S7 for 40 min in 50% KOH solution. Longer etching times and higher KOH concentration are expected to lead to smoother sidewalls and narrower grating bars. Without destroying the samples SEM images let us determine the width of grating bars at the top and bottom of the device layer. Spot checking with the SEM we do not find a clear trend for grating bar widths across the samples - they all appear to be around 60 nm wide at the top. Reduced sidewall roughness should result in higher diffraction efficiency, but instead we find that samples S1 and S3 performed the best (see Fig. 7(b)). We also

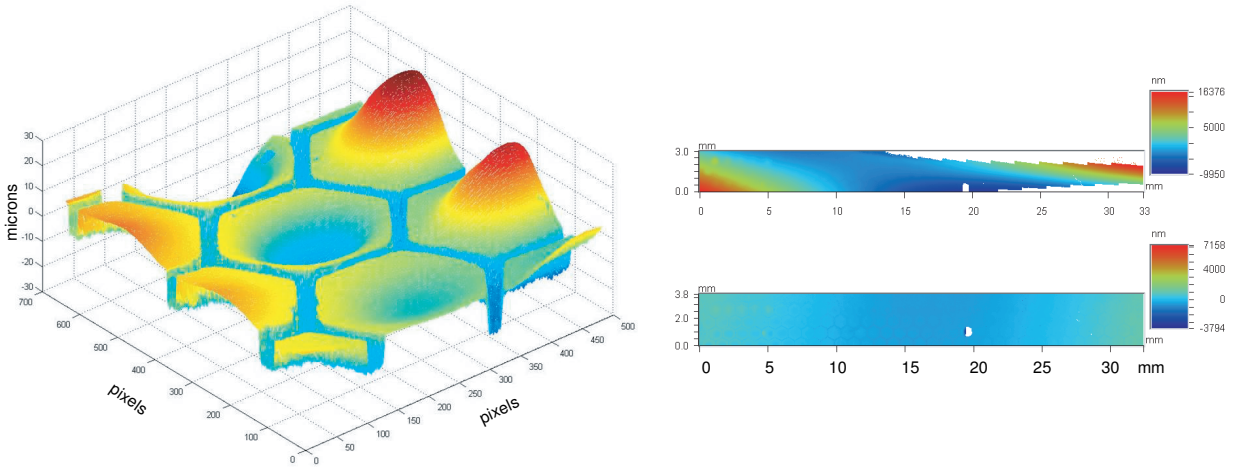

Figure 6. Left: Cutout of device layer topography of sample B2 measured with optical profiler. A pixel corresponds to ~ 3.6 μm. The device layer for some hexagons is buckled by several microns up or down, while for other hexagons it remains quite flat. (The height values for the device layer on top of the L2 mesh are an artefact, probably due to the partial transparency of the CAT grating layer for visible light.) Right, top: Topography of sample S6, while held by clips against its aluminum sample mount, showing bending by more than 30 microns. Right, bottom: Topography of sample S6, after clips have been removed. The sample is bent by less than two microns.

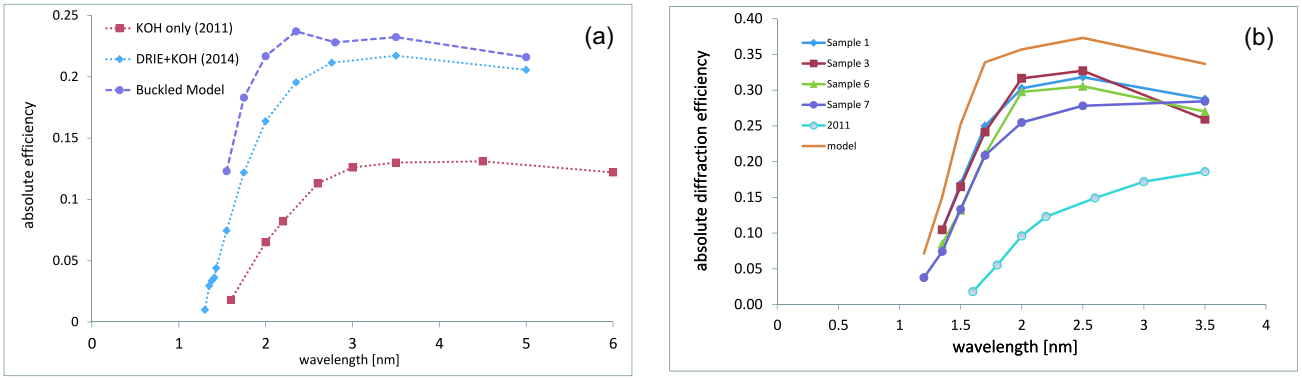

Figure 7. (a) Absolute diffraction efficiency of the strongest blazed order as a function of wavelength. "KOH only" shows measured efficiencies for the best sample produced via wet etch alone with $\alpha \sim 2.6$ deg.[18] "DRIE + KOH" refers to measurements of a single spot on sample B2 with $\alpha = 2.23$ deg. "Buckled model" is the theoretical efficiency that would be expected of a perfect CAT grating with similar parameters as B2 and with the measured buckling of the same spot where the B2 x-ray data was taken, also for $\alpha = 2.23$ deg. (b) Sum of absolute diffraction efficiencies from orders under the blaze envelope. "2011" refers to the same wet-etched sample as in (a) with $\alpha \sim 2.6$ deg.[18] Sample 1-Sample 7 refers to the samples from the most recent batch with $\alpha = 1.91$ deg. "Model" refers to the theoretical efficiency for the same orders for a perfect CAT grating with similar geometrical parameters as samples S1-S7, also for $\alpha = 1.91$ deg.

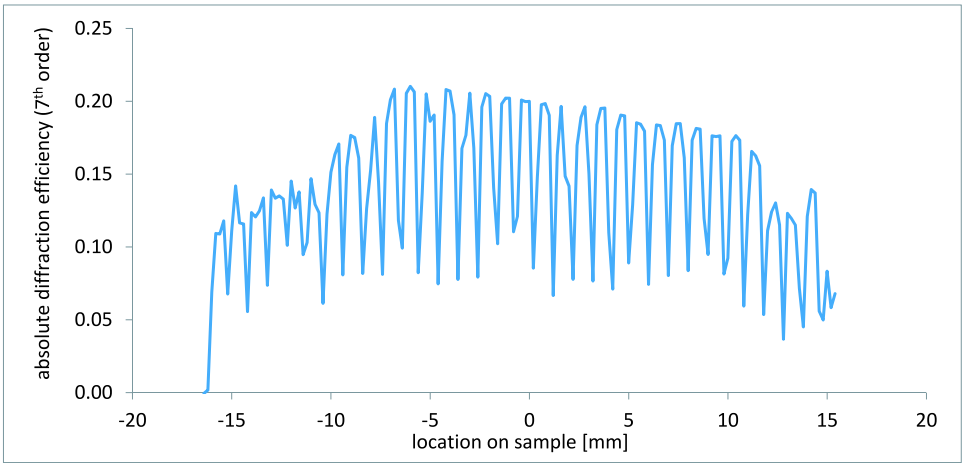

Figure 8. Absolute diffraction efficiency of 7^{th} order along a straight line across sample S1 for $\lambda = 2$ nm and $\alpha = 2$ deg. The periodic dips in efficiency are due to absorption by the L2 mesh.

observe more defects in samples S6 and S7, which might indicate that the longer KOH etch thins and weakens the grating bars and thus makes them more susceptible to mechanical damage. Samples S1 and S3 performed in the range of 70-90 % of model predictions.

The data shown in Figs. 5 and 7 were all taken over single areas on each sample, corresponding to the footprint of the x-ray beam, and avoiding L2 mesh bars. However, for large-area samples it is important to have high diffraction efficiency over the whole sample. In order to characterize a whole sample we center the detector on a blazed diffraction peak and scan the sample in its own plane along a straight line, maintaining a constant angle between the sample mount and the beam. An example of such a scan is shown in Fig. 8. The diffraction efficiency is relatively high for most of the sample, but it falls off towards the edges. In many cases we can recover close to the highest observed efficiency in areas of weaker diffraction through small changes in α (a few tenths of a degree or less). This indicates that our sample might not be flat across its length ($\sim$ 33 mm). We were able to confirm this assumption with the optical profiler. As shown on the right in Fig. 6, sample S6 is bent by tens of micrometer when clamped to its x-ray mount, but springs back to almost completely flat when it is released from the clamps. We found similar deformations for samples S1 and S3. On the scale of individual hexagons we observed only rather mild to negligible buckling in the latest batch, especially when compared to sample B2.

5. DISCUSSION

We have obtained record-high absolute diffraction efficiencies from our recently fabricated CAT grating samples, almost doubling it through the combination of anisotropic dry and wet etching. Our yields have improved through process and handling improvements, and our fabrication results have become more consistent and repeatable. However, there is still room for further improvement. Compared to theory based on rigorous coupled-wave analysis,[32] CAT gratings perform better towards longer wavelengths and worse towards the critical wavelength (where the angle of incidence α approaches the critical angle $\theta_c(\lambda)$). This is usually a sign of structural imperfection, but from our data it is difficult to say anything about the spatial scale of potential imperfections. The typical defects discernible with SEM imaging are grating bars that are stuck together or broken. Microroughness on the grating bar sidewalls with spatial scales below the SEM resolution ($\sim 2-5$ nm) can also contribute to the observed behavior. Longer etching in KOH is expected to reduce sidewall roughness, but it will eventually thin all the silicon structures. From our comparison of samples S1, S3, S6, and S7 we find that the samples with the shortest KOH etch times perform the best, but this could be due to the noticeably higher defect density in samples S6 and S7. For S7 only a few hexagons survived with intact CAT gratings, and for most hexagons the device layer had simply vanished. In the future we want to create gratings with higher duty cycle that can be etched longer in KOH without losing too much mechanical strength. There is a trade-off between the strength of thicker bars and the reduced x-ray absorption with thinner bars. Strength is mostly required to survive fabrication. Once the gratings are finished we have not observed new defects from reasonable

handling of the samples. Thus it might make sense to gently thin grating bars post fabrication, using iterations of thermal oxidation and oxide removal through HF vapor etching.

Future CAT grating batches will employ an additional integrated L2 mesh in the device layer that is aligned with the back side L2 mesh. This should allow us to perform long and thorough HF etches without the danger of delamination and decrease of membrane strength.

We have not yet performed a detailed comparison of sample deformation in the x-ray mount and observed efficiency variations as in Fig. 8, but the derived angle variations are of the same order of magnitude for both types of data (tenths of degrees). We will therefore design improved sample mounts to avoid sample deformation.

In this work we have compared measured soft x-ray diffraction efficiencies with theoretical predictions for ideal gratings with the same geometrical parameters (p, d, b) as the fabricated gratings. Significantly higher efficiencies ($> 50\%$ absolute efficiency, including L1 absorption) are predicted for more challenging geometries, such as smaller grating bar duty cycle and deeper gratings (up to 6 μm) at smaller angles of incidence.[11] We have already demonstrated such geometries with KOH etching,[18] and it is conceivable that we can also realize them with our current process. Additional throughput is possible through reduced duty cycles for L1 and L2 supports.

6. FUTURE PLANS

Our next goal is to demonstrate CAT grating resolving power in an x-ray imaging system, such as the one at the Marshall Space Flight Center Stray Light Test Facility.[33,34] The dominant limiting factor (apart from the telescope point-spread function (PSF)) in achieving $R \sim 3000$ for a CAT grating spectrometer is the variation in grating period. Instead of a test which involves an x-ray imaging system one could more easily directly measure period variation over the whole area of a grating facet with a technique similar to the one used for the transmission gratings for Chandra.[35] We are studying the possibility of integrating such a technique into our Nanoruler grating patterning and metrology tool.[36]

We will investigate extending CAT grating performance towards higher energies and/or diffraction angles by coating the silicon bars with a high-Z metal using atomic layer deposition.

Detailed ray tracing has been done for several CATXGS designs that assumed telescope angular resolution in the range of 5-10 arcsec, and demonstrated the feasibility of reaching $R > 3000$.[6,7,11,13] In these cases the resolving power was limited by the telescope PSF. For a future X-ray Surveyor with a half-arcsec PSF this will not be the case, and previously negligible terms in the resolving power error budget will become important. Preliminary ray tracing simulations in the context of the Smart-X concept[14] indicate that achieving $R \sim 5000$-6000 should be a rather straightforward possibility. We intend to investigate the error budget and limits for R for an X-ray Surveyor-type mission in the near future.

7. SUMMARY

An x-ray grating spectrometer with large collecting area is the instrument of choice to move forward the science of high-resolution soft x-ray spectroscopy in astrophysics. An XGS based on CAT gratings offers synergy with a microcalorimeter, minimal spacecraft resource requirements, and competitive performance. We have improved CAT grating performance by almost a factor of two and demonstrated over 30% diffraction efficiency in the soft x-ray band. Further process development, as well as development of mounting and alignment schemes for large grating arrays will mature technology for a future CATXGS towards higher TRLs in a timely fashion.

ACKNOWLEDGMENTS

We gratefully acknowledge support from E. Gullikson (ALS), F. DiPiazza (Silicon Resources), Martin Klingensmith and Brandon Chalifoux (both SNL), and facilities support from the Nanostructures Laboratory and the Microsystems Technology Laboratories (both at MIT). This work was performed in part at the Advanced Light Source at Lawrence Berkeley National Lab, which is supported by the Director, Office of Science, Office of Basic Energy Sciences, of the U.S. Department of Energy under Contract No. DE-AC02-05CH11231. This work was supported by NASA grants NNX12AF21G and NNX15AC43G.

REFERENCES

[1] Bautz, M. W. *et al.*, "AEGIS - an astrophysics experiment for grating and imaging spectroscopy," Response to NASA solicitation NNH11ZDA018L, http://pcos.gsfc.nasa.gov/studies/rfi/Bautz-Marshall-RFINNH11ZDA018L.pdf (2011).

[2] "New Worlds, New Horizons in Astronomy and Astrophysics," National Research Council, http://www.nap.edu/catalog.php?record_id=12951 (2010).

[3] "Enduring Quests, Daring Visions," NASA 2013 Astrophysics Roadmap, http://science.nasa.gov/media/medialibrary/2013/12/20/secure-Astrophysics_Roadmap_2013.pdf

[4] Canizares, C. R. *et al.*, "The Chandra high-energy transmission grating: Design, fabrication, ground calibration, and 5 years in flight," *PASP* **117**, 1144-1171 (2005).

[5] den Herder, J. W. *et al.*, "The reflection grating spectrometer on board XMM-Newton," *Astr. & Astroph.* **365**, L7-L17 (2001).

[6] Bautz, M. W. *et al.*, "Concepts for high-performance soft x-ray grating spectroscopy in a moderate-scale mission," *Proc. SPIE* **8443**, 844315 (2012).

[7] Davis, J. E., Bautz, M. W., Dewey, D., Heilmann, R. K., Houck, J. C., Huenemoerder, D. P., Marshall, H. L., Nowak, M. A. and Schattenburg, M. L., "Raytracing with MARX - X-ray observatory design, calibration, and support," *Proc. SPIE* **8443**, 84431A (2012).

[8] NASA X-ray Mission Concepts Study Project Report, http://pcos.gsfc.nasa.gov/physpag/X-ray_Mission_Concepts_Study_Report-Final.pdf

[9] Smith, R. K. *et al.*, "Arcus: An ISS-attached high-resolution x-ray grating spectrometer," *Proc. SPIE* **9144**, 91444Y (2014).

[10] Bookbinder, J., "An overview of the IXO Observatory," *Proc. SPIE* **7732**, 77321B (2010).

[11] Heilmann, R. K. *et al.*, "Critical-angle transmission grating spectrometer for high-resolution soft x-ray spectroscopy on the International X-Ray Observatory," *Proc. SPIE* **7732**, 77321J (2010).

[12] McEntaffer, R. L. *et al.*, "Development of off-plane gratings for WHIMex and IXO," *Proc. SPIE* **8147**, 81471K (2011).

[13] Bookbinder, J. A. *et al.*, "The Advanced X-ray Spectroscopic Imaging Observatory (AXSIO)," *Proc. SPIE* **8443** 844317 (2012).

[14] Vikhlinin, A. *et al.*, "SMART-X: Square Meter Arcsecond Resolution X-Ray Telescope," *Proc. SPIE* **8443** 844316 (2012).

[15] Hertz, P., "Planning for the 2020 Decadal Survey: An Astrophysics Division White Paper," http://science.nasa.gov/astrophysics/documents

[16] Weisskopf, M. C, Gaskin, J., Tananbaum, H. and Vikhlinin, A., "Beyond Chandra: the X-ray Surveyor," *Proc. SPIE* **9510**, 951002 (2015).

[17] Gaskin, J. *et al.*, "The X-ray Surveyor Mission: A Concept Study," Proc. SPIE **9601**, to be published.

[18] Heilmann, R. K., Ahn, M., Bruccoleri, A., Chang, C.-H., Gullikson, E. M., Mukherjee, P. and Schattenburg, M. L., "Diffraction efficiency of 200 nm period critical-angle transmission gratings in the soft x-ray and extreme ultraviolet wavelength bands," *Appl. Opt.* **50**, 1364-1373 (2011).

[19] Heilmann, R. K. *et al.*, "Critical-angle transmission gratings for high resolution, large area soft x-ray spectroscopy," Response to NASA solicitation NNH11ZDA018L, http://pcos.gsfc.nasa.gov/studies/rfi/Heilmann-Ralf-RFINNH11ZDA018L.pdf (2011).

[20] Heilmann, R. K., Ahn, M., Gullikson, E. M. and Schattenburg, M. L., "Blazed high-efficiency x-ray diffraction via transmission through arrays of nanometer-scale mirrors," *Opt. Express* **16**, 8658-8669 (2008).

[21] Heilmann, R. K., Ahn, M. and Schattenburg, M. L., "Fabrication and performance of blazed transmission gratings for x-ray astronomy," *Proc. SPIE* **7011**, 701106 (2008).

[22] Ahn, M., Heilmann, R. K. and Schattenburg, M. L., "Fabrication of ultrahigh aspect ratio freestanding gratings on silicon-on-insulator wafers," *J. Vac. Sci. Technol. B* **25**, 2593-2597 (2007).

[23] Ahn, M., Heilmann, R. K. and Schattenburg, M. L., "Fabrication of 200 nm-period blazed transmission gratings on silicon-on-insulator wafers," *J. Vac. Sci. Technol. B* **26**, 2179-2182 (2008).

[24] Heilmann, R. K. *et al.*, "Development of a critical-angle transmission grating spectrometer for the International X-Ray Observatory," *Proc. SPIE* **7437**, 74370G (2009).

[25] Heilmann, R. K., Bruccoleri, A., Mukherjee, P., Yam, J. and Schattenburg, M. L., "Fabrication update on critical-angle transmission gratings for soft x-ray grating spectrometers," *Proc. SPIE* **8147**, 81471L (2011).

[26] Heilmann, R. K., Bruccoleri, A., Mukherjee, P. and Schattenburg, M. L., "Progress in the Development of Critical-Angle Transmission Gratings," *Proc. SPIE* **8443**, 84430W (2012).

[27] Bruccoleri, A., Mukherjee, P., Heilmann, R. K., Yam, J. and Schattenburg, M. L., "Fabrication of nanoscale, high throughput, high aspect ratio freestanding gratings," *J. Vac. Sci. Technol. B* **30** 06FF03 (2012).

[28] Mukherjee, P., Bruccoleri, A., Heilmann, R. K., Schattenburg, M. L., Kaplan, A. F. and Guo, L. J.,"Plasma etch fabrication of 60:1 aspect ratio silicon nanogratings on 200 nm pitch," *J. Vac. Sci. Technol. B* **28**, C6P70-5 (2010).

[29] Bruccoleri, A. R., Guan, D., Vargo, S., DiPiazza, F., Heilmann, R. K. and Schattenburg, M. L., "Nanofabrication advances for high efficiency critical-angle transmission gratings," *Proc. SPIE* **8861**, 886119 (2013).

[30] Bruccoleri, A. R., Guan, D., Mukherjee, P., Heilmann, R. K., Schattenburg, M. L. and Vargo, S., "Potassium hydroxide polishing of nanoscale deep reactive-ion etched ultra-high aspect ratio gratings," *J. Vac. Sci. Technol. B* **31**, 06FF02 (2013).

[31] Heilmann, R. K., Bruccoleri, A. R., Guan, D. and Schattenburg, M. L., "Fabrication of large-area and low mass critical-angle x-ray transmission gratings," *Proc. SPIE* **9144**, 91441A (2014).

[32] Moharam, M. G., Pommet, D. A., Grann, E. B., Gaylord, T. K., "Stable implementation of the rigorous coupled-wave analysis for surface-relief gratings - enhanced transmittance matrix approach," *J. Opt. Soc. Am. A* **12**, 1077-1086 (1995).

[33] Zhang, W. W., *et al.*, "Next generation astronomical x-ray optics: high angular resolution, light weight, and low production cost," *Proc. SPIE* **8443**, 84430S (2012).

[34] McEntaffer, R., *et al.*, "First results from a next-generation off-plane X-ray diffraction grating," *Exp. Astron.* **36**, 389 (2013).

[35] Dewey, D., Humphries, D. N., McLean, G. Y. and Moschella, D. A., "Laboratory calibration of x-ray transmission diffraction gratings," *Proc. SPIE* **2280**, 257 (1994).

[36] Heilmann, R. K., Chen, C. G., Konkola, P. T. and Schattenburg, M. L., "Dimensional metrology for nanometer-scale science and engineering: Towards sub-nanometer accurate encoders," *Nanotechnology* **15**, S504 (2004).